2D surface wave inversion : $MultioffsetMASWvs.FWI$

Luping Qu, Wenyong Pan, Jan Dettmer, Kris Innanen

ABSTRACT

Two major methods for 2D near-surface investigation are the Multi-offset MASW (MO-MASW) and surface-wave full waveform inversion. We test these two methods and analyze their limitations and advantages. MO-MASW can roughly detect and locate the abrupt lateral variation. However, it has difficulties in resolving irregular anomalous bodies or complex subsurface velocity structure. Full waveform inversion method overcomes these problems by providing a detailed subsurface shear-wave velocity structure, but easy to fall into local minimum since surface wave has a shorter wavelength. We test the surface wave full waveform inversion method on synthetic models containing high-velocity and low-velocity anomalous bodies. To avoid the cycle skipping, misfit function, combining waveform-difference and envelop-difference, is adopted, and a frequency-decreasing multi-scale approach is incorporated. From our synthetic tests, we find besides the negative and positive velocity anomalies, the nested velocity anomalies can be well recovered as well. At last, a preliminary test on surface-trenched DAS data is conducted using this multi-scale full waveform inversion process.

INTRODUCTION

Since the layer-model assumption is made for multichannel analysis of surface wave (MASW), inverted shear-wave velocity is averaged over the line of whole receivers. Therefore, obtained results where lateral variations exist cannot be treated reliable. This problem leads to the multi-offset phase analysis (MOPA) of the surface wave. Through a preliminary multi-offset analysis combined with seismogram, the abrupt lateral variations can be identified. Then, dispersion curve picking and inversion can be done on two sides of the discontinuity separately. The feasibility of using MOPA for abrupt lateral variation has been proved in previous study (Strobbia and Foti, 2006; Vignoli and Cassiani, 2010; Mastrocicco et al., 2010). Effect of dipping layer on seismic surface waves profiling has been studied numerically (Bodet et al., 2004). In these studies, only simple velocity structures, like a single dipping layer, rectangular velocity anomalous body, or a fault are tested. However, any complex structures or combinations of these cannot be well characterized using this conventional approach. When the model structure is complex, the corresponding seismogram will be complicated as well, hard to separate into several parts horizontally. Besides, the picking of dispersion curves will be another challenge. Thus, the multi-offset multichannel analysis of surface wave can account for the lateral variations to some degree, but can not resolve complex velocity structures.

The accuracy of near-surface velocity structure determination is significant for seismic imaging in the deep area. Thus, geophysicists have turned their attention to the full waveform inversion (FWI) method. As surface wave dominates the shallow site, the study on surface wave full waveform inversion is naturally conducted (Borisov et al., 2018; Pan et al., 2019). Surface waves have several differences from the body waves in the property. The propagation of surface waves in a vertically heterogeneous medium is characterized by

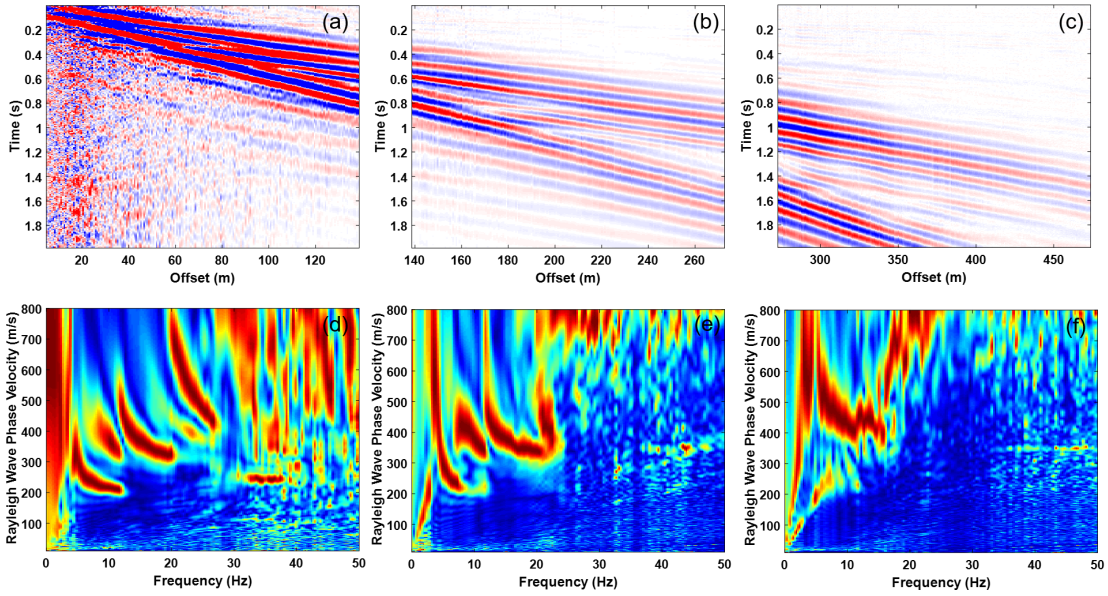

FIG. 1. A sample for multi-offset analysis of the DAS data.

dispersion, which means different frequencies propagate along with different depths and with different phase velocities. As the surface wave is particularly sensitive to shear-wave velocity, the inversion results are mainly shear-wave velocities. Due to the low velocity and dispersion characteristic, the surface wave inversion is easily trapped in local minimum (Romdhane et al., 2011). Simultaneous multi-frequency inversion, envelop-based misfit function, the layer-stripping approach can be adopted to diminish the dependence on the initial model and avoid cycle skipping. Raul developed a multi-step surface wave inversion method by decomposing the multimode surface wave in advance (Cova and Innanen, 2019), and conduct the inversion from fundamental mode to higher modes, which can improve the resolution of the results. Here we tested these methods above using synthetic models. For the synthetic data, we first use the envelop-based misfit function to determine the large scale structures. Following this, we use the waveform-difference misfit function to obtain the final inversion result. As for the field data, which is the surface-trenched DAS data, we first use the cross-correlation travel time objective function to do an initial inversion, and then we use the waveform-difference objective function for the subsequent inversion. The frequency-decreasing multi-scale approach is conducted during all these inversions.

MULTI-OFFSET PHASE ANALYSIS

To implement multi-offset phase analysis, firstly, we need to do an overlapping multi-offset analysis. To increase the lateral resolution, the trace number of each offset should be small enough, as the results are averaged over the offset. Meanwhile, the clearance of the dispersion curves can be influenced by the trace number. Thus, it is a trade-off parameter, which we should decide based on the data quality. Here, ten overlapping offsets with 200 traces are used to cover the whole data offset.

Here, a sketch of multi-offset analysis is shown in FIG. 1. In practice,10 overlapping offsets are selected. The corresponding dispersion curves are picked from the frequency

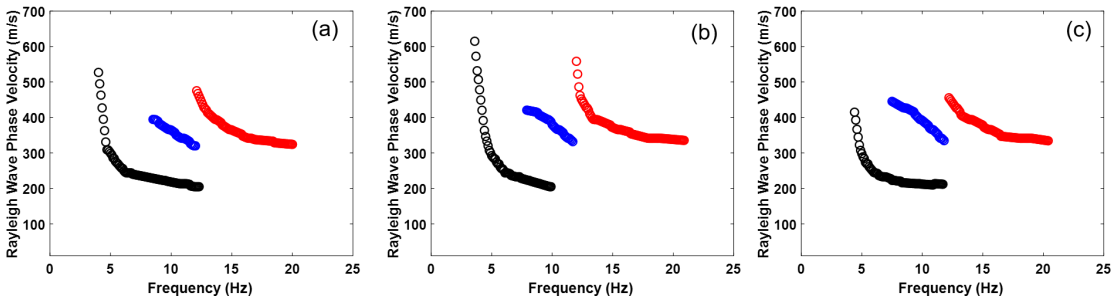

FIG. 2. Three samples of dispersion curves picked from the multi-offset spectrum.

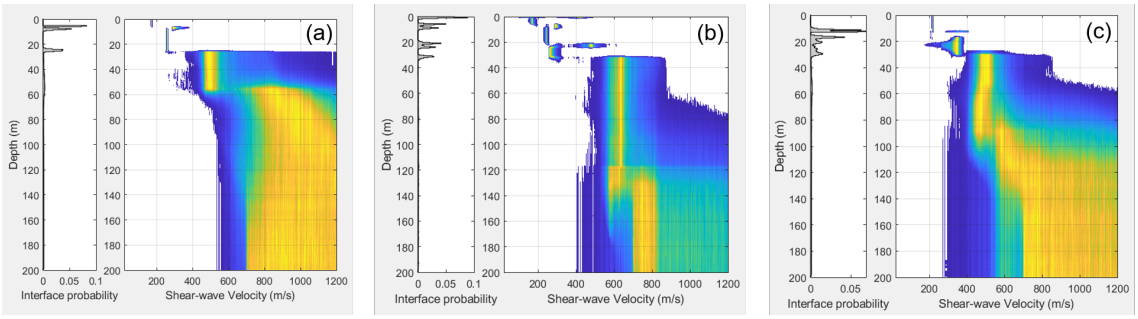

FIG. 3. Inversion results for the dispersion curves in FIG. 2.

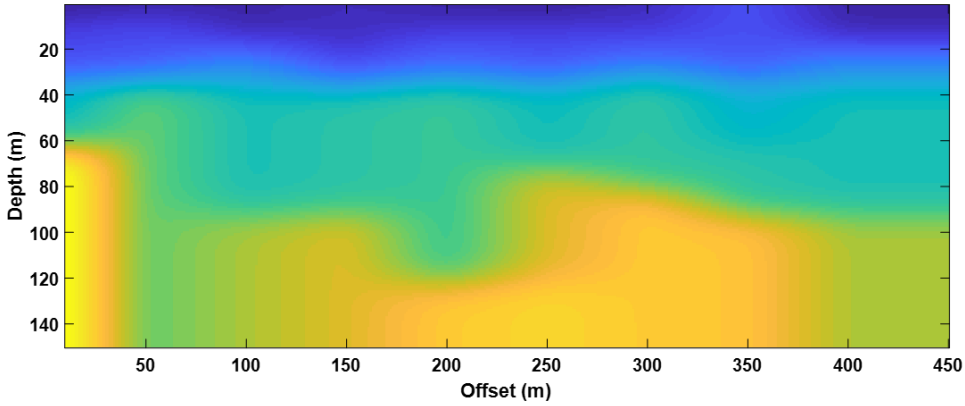

FIG. 4. Subsurface imaging using 2D interpolation of 1D shear-wave velocity inversion results .

spectra. For lack of space, only three samples of dispersion curves (FIG. 2) and their inversion results (FIG. 3) are shown. The multimode dispersion curves surface wave inversion using the trans-dimensional inversion method is adopted. Finally, 2D interpolation is conducted based on these 1D results (FIG. 4). From FIG. 3, we can find there is a comparatively small shear-wave velocity uncertainty at the depth within around 50 m. The uncertainty beyond 50 m is considerable. Therefore, the shear-wave velocity at the shallow part in FIG. 4 is more reliable than the deeper part. For this test, due to the large uncertainty in 1D results, the velocity structure below 100 m may not be accurate.

Based on literature reviews and synthetic tests, it is easily found that the MOPA has limited ability in resolving complex lateral heterogeneities. Simple laterally variational structures like faults or regular-shaped anomalous velocity body can be detected and located through this process. However, complex lateral structures are hard to detect and resolve, especially due to the averaging effect. To improve the near-surface imaging resolution, advanced imaging methods and extra data information should be utilized.

SURFACE-WAVE FULL WAVEFORM INVERSION

Compared with finite-difference, the spectral element method has advantages in model-meshing flexibility. In this study, the spectral-element based wave propagation solver is used for forward simulation. To demonstrate the FWI inversion method for resolving lateral variations, two synthetic models are created. Both of them have positive and negative velocity anomalous bodies in square shape and circle shape. The difference is the second model includes two nested round velocity anomalies. This type of velocity structure is hard to resolve using reflected waves. However, in surface wave FWI, it is possible to resolve this type of velocity structure. Since surface wave haS short wavelength and dispersion characteristic, it suffers from cycle skipping greater than body wave. There are several methods dealing with the cycle skipping in surface-wave FWI, such as changing misfit function and layer stripping strategy. For the data misfit measurements, besides the conventional L2-norm waveform-difference misfit, envelop-different misfit function is also tested and combined in the synthetic test. L-BFGS is adopted to compute search direction. The conventional waveform difference objective function is

$$\chi^{\mathrm{WD}} = \frac{1}{2}\left[u_i - u_i^{\mathrm{obs}}\right]^2. \tag{1}$$

The corresponding adjoint source $\tilde{f}^{\dagger}_{i,\mathrm{WD}}$ is

$$\tilde{f}^{\dagger}_{i,\mathrm{WD}} = u_i - u_i^{\mathrm{obs}}. \tag{2}$$

Envelop measures the instantaneous amplitude of seismic signal (Bozdağ et al., 2011). The envelope of the seismic data $f(t)$ is calculated as

$$E_i = \sqrt{f^2(t) + \mathcal{H}\{f(t)\}^2} \tag{3}$$

which is also a function of time. The envelop-difference misfit function is

$$\chi^{\mathrm{ED}} = \frac{1}{2}\left[E_i - E_i^{\mathrm{obs}}\right]^2, \tag{4}$$

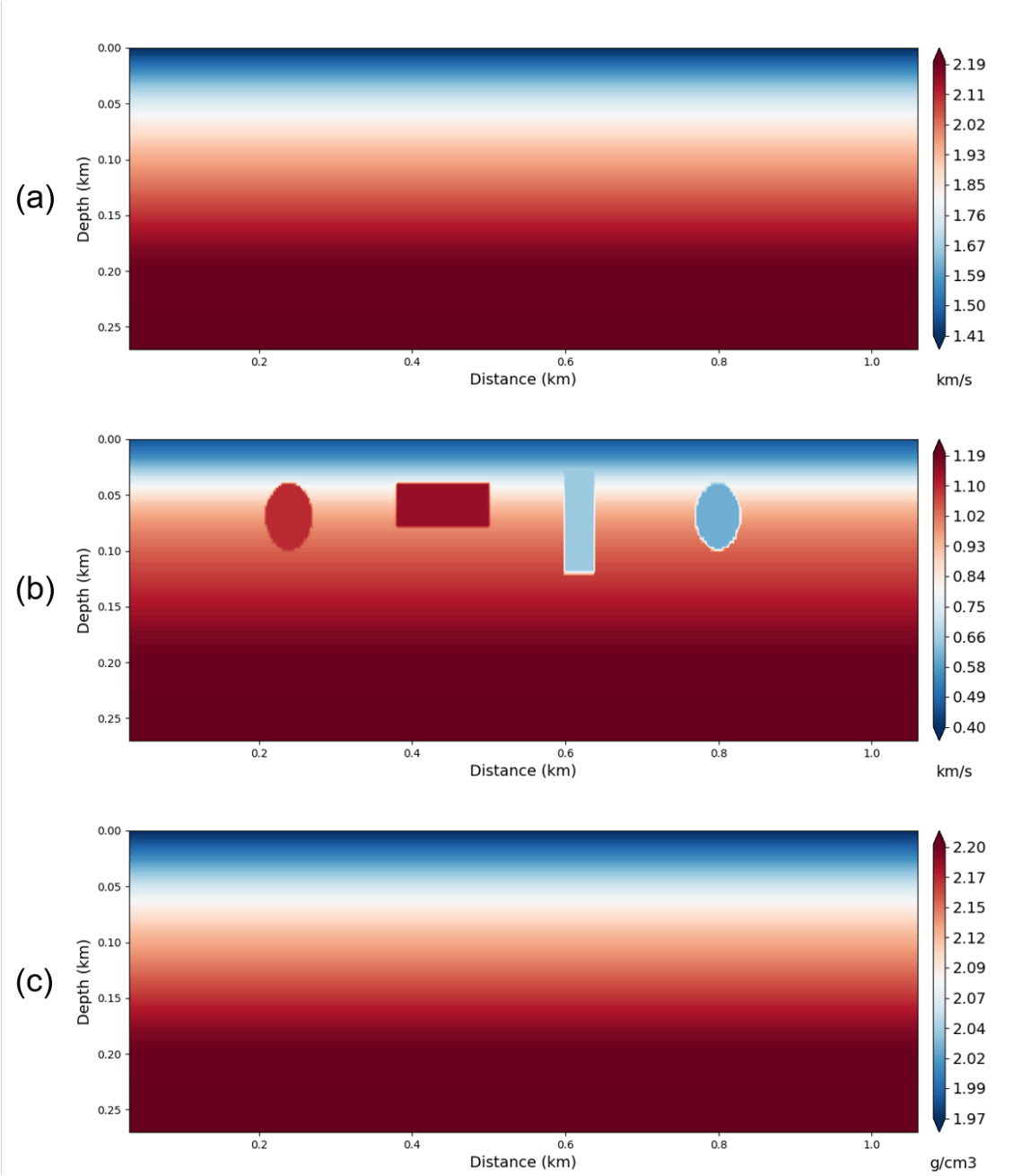

FIG. 5. (True velocity and density model.(a) Vp model. (b) Vs model. (c) Density model.

where E_i is the envelope of the seismic data. The adjoint source is

$$\tilde{f}^{\dagger}_{i,\mathrm{ED}} = \frac{E_i - E_i^{\mathrm{obs}}}{E_i} u_i - \mathcal{H}\left[\frac{E_i - E_i^{\mathrm{obs}}}{E_i}\mathcal{H}\left[u_i\right]\right], \tag{5}$$

where $\mathcal{H}$ represents the Hilbert transform. A wavelet and its envelope have different effective bandwidths. Therefore, they can be exploited to minimize cycle skipping and increase resolution based on the half-wavelength continuity criterion. Seismic envelope inversion methods can utilize the low-frequency components from the original seismic data for FWI, by using the nonlinear demodulation operator, and the initial model dependence in waveform inversion is reduced. The adjoint source of envelope-based inversion is related to waveform and envelope data, while the adjoint source of conventional FWI is determined by waveform (Luo and Wu, 2015). Besides, Luo and Wu (2015)'s research also shows the noise resistance ability of envelope inversion to Gaussian noise and seismic interference noise is robust.

Numerical examples

The first synthetic model is a model, including positive and negative velocity anomalous bodies in square shape and round shape. True Vp, Vs, and density models are displayed in FIG. 5. A total of 20 shots are positioned by a 50-m interval on the surface, and the receiver point number is 210 with a interval of 5 m. Ricker wavelet with a dominant frequency of 10 Hz is used for forward simulations. The initial Vs model is shown in FIG. 6. To minimize

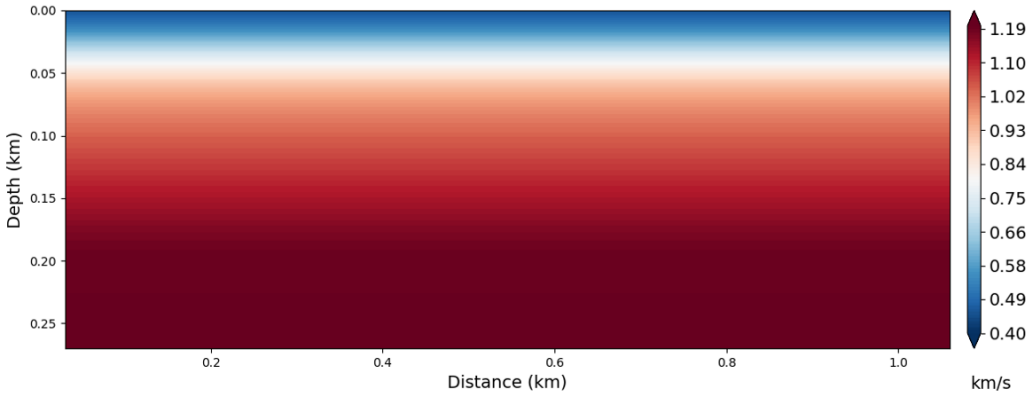

FIG. 6. Initial Vs model.

the cycle skipping, for the first 20 iterations inversion, we use the envelop-based FWI from an linear initial model. And for the subsequent 20 iterations, we use the waveform-difference misfit function. The initial shear-wave velocity inversion result is displayed in FIG. 7. Thus, a smooth background model with large-scale structures is obtained. FIG. 8 shows the final result of combined inversion (ED+WD FWI). Both the positive and negative velocity anomalies in different shapes are fully recovered.

Another synthetic test is done on an interesting model shown in FIG. 9 (a). In this model, two nested velocity anomalies are included. One circular low-velocity anomaly

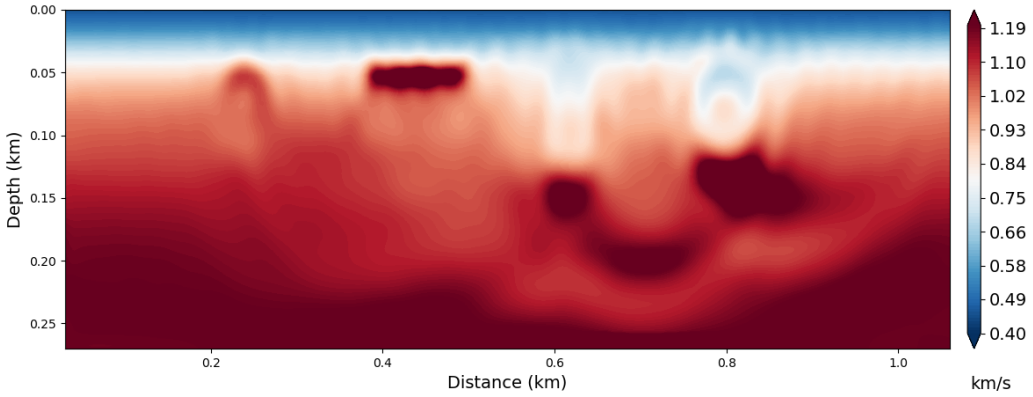

FIG. 7. Shear wave velocity model obtained after the first 20 iterations using envelope-difference misfit function.

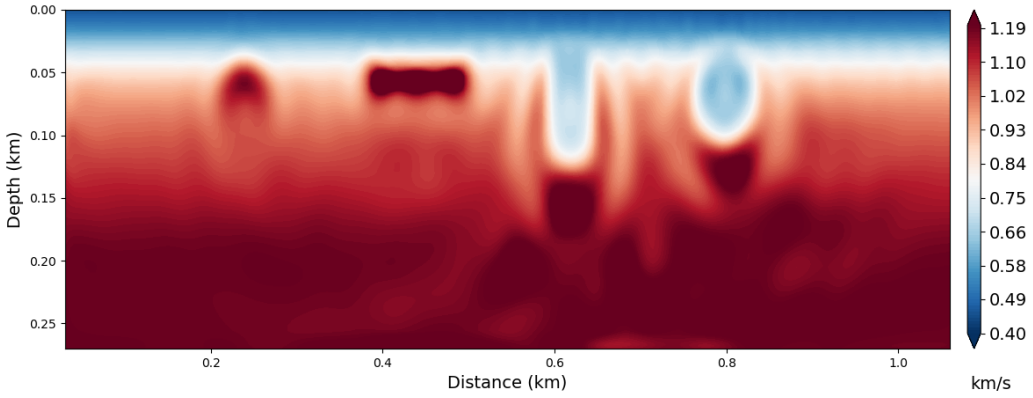

FIG. 8. Shear wave velocity model obtained after 40 iterations.

encapsulated by a circular high-velocity anomaly is placed in the left of the synthetic model. One circular high-velocity anomaly encapsulated by a circular low-velocity anomaly is placed in the right of the model. We want to test how well this structure can be resolved using the combined misfit FWI. A total 20 shots are positioned by a 40-m interval on the surface, and the receiver point number is 180 with an interval of 5 m. Ricker wavelet with a dominant frequency of 10 Hz is used for forward simulations. The Vp and density models are linear models similar to the first synthetic test. Therefore, only the shear-wave velocity true model, the initial model, and inversion result are shown (FIG. 9).

With reflected wave FWI, it is difficult to resolve this type of nested velocity model. But using multi-scale surface-wave FWI, this type of velocity structure can be well recovered. This is related to the propagation path of surface waves. Solution non-uniqueness still exist, which can be seen from the recovering of the rectangular low-velocity anomaly in FIG. 9 (c). Developments on the current algorithm should be further studied.

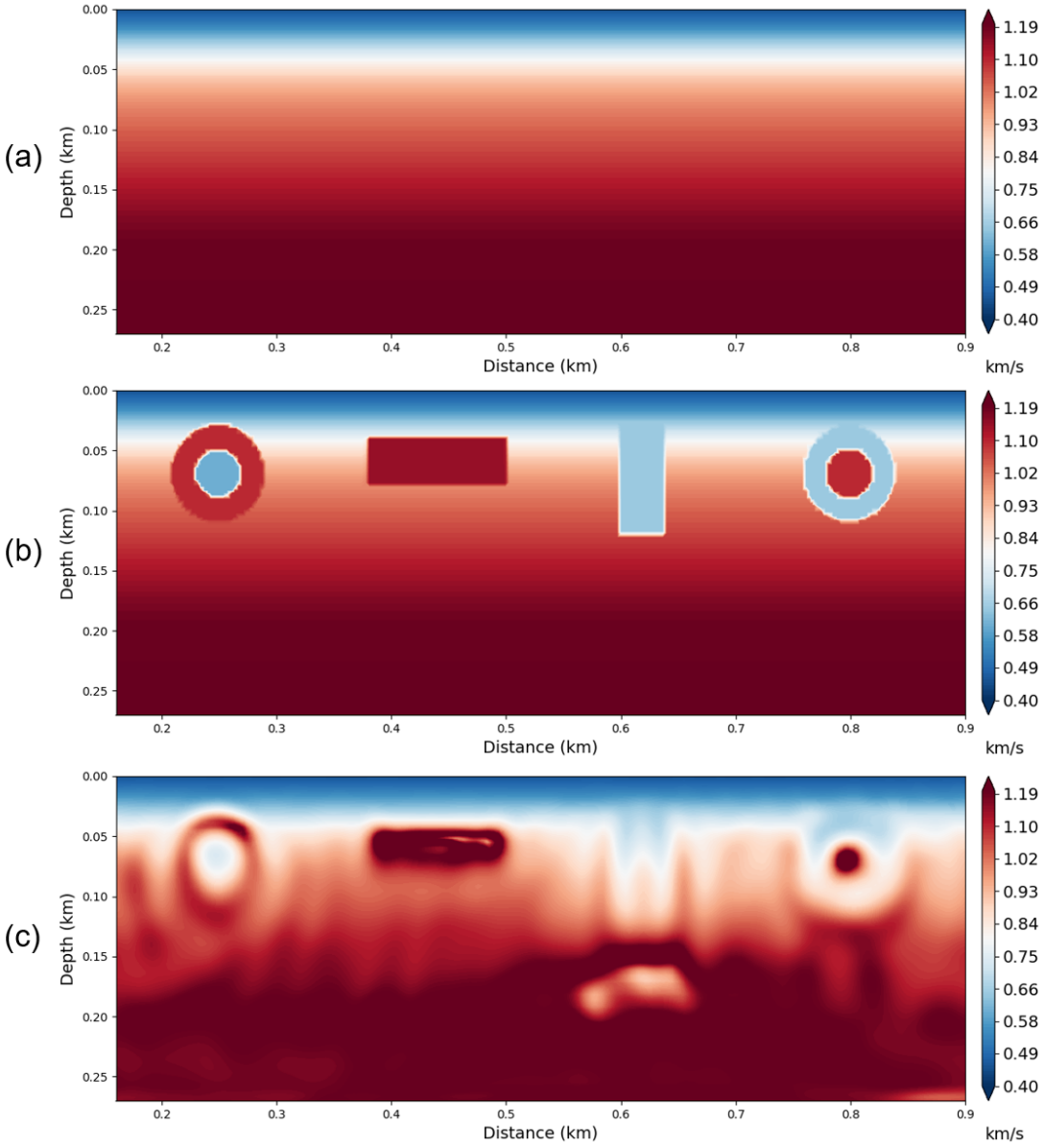

FIG. 9. Shear wave velocity model. (a) True Vs model. (b) Initial Vs model. (c) Inverted Vs model.

Application to DAS data

DAS measures the distance change of impurities in the fibre due to the wavefield propagation. In practice, DAS systems measure the distance length change (i.e. strain) over a piece of fibre, so that the energy of the backscattered lasers are enhanced. To implement DAS data FWI, we need to transform the measurement data from strain to displacement at first.

$$\epsilon'(r) = \frac{1}{L_g}(u(r + \frac{L_g}{2}) - u(r - \frac{L_g}{2})) \tag{6}$$

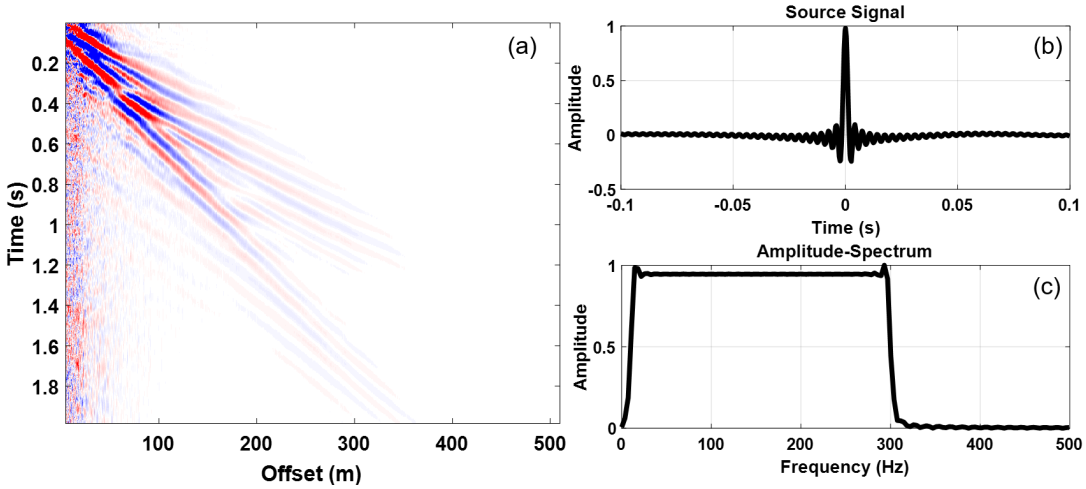

FIG. 10. Observing data and Klauder wavelet. (a) Observing DAS data. (b) Klauder wavelet. (c) frequency spectrum of the wavelet.

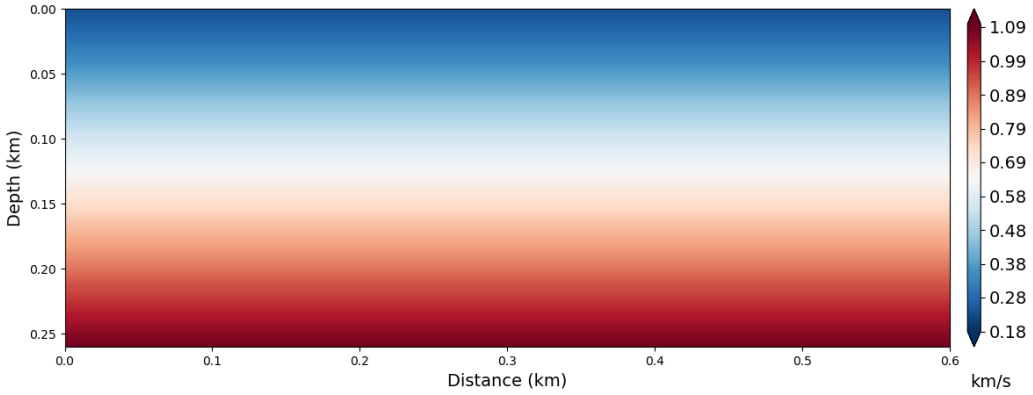

FIG. 11. Initial model for FWI.

where $\epsilon'(r)$ is the strain at r, u is displacement, and L_g is the gauge length. Therefore, the relationship of $\epsilon'(r)$ and displacement u can be characterized using the following equation.

$$\begin{pmatrix} \epsilon'_1 \\ \epsilon'_2 \\ \vdots \\ \epsilon'_N \end{pmatrix} = \begin{pmatrix} -1 & 1 & & & \\ & -1 & 1 & & \\ & & \ddots & \ddots & \\ & & & -1 & 1 \end{pmatrix} \begin{pmatrix} u_1 \\ u_2 \\ \vdots \\ u_M \end{pmatrix}. \tag{7}$$

This is actually an under-determined problem, as the displacement vector has more freedom than the strain vector. Therefore, SVD is used to transform the data. Another important issue to keep the synthetic data and observing data consistent is the wavelet. The amplitude and phase of the wavelet can influence the generated waveform greatly. The data we use is generated from the vibroseis source. Therefore the wavelet for FWI is the Klauder wavelet with the time step of 0.0002 s, shown in FIG. 10 (b) and (c).

At present, the absorbing attenuation has not been considered, so preliminary processings such as the automatic amplitude gaining and normalization are conducted on both the

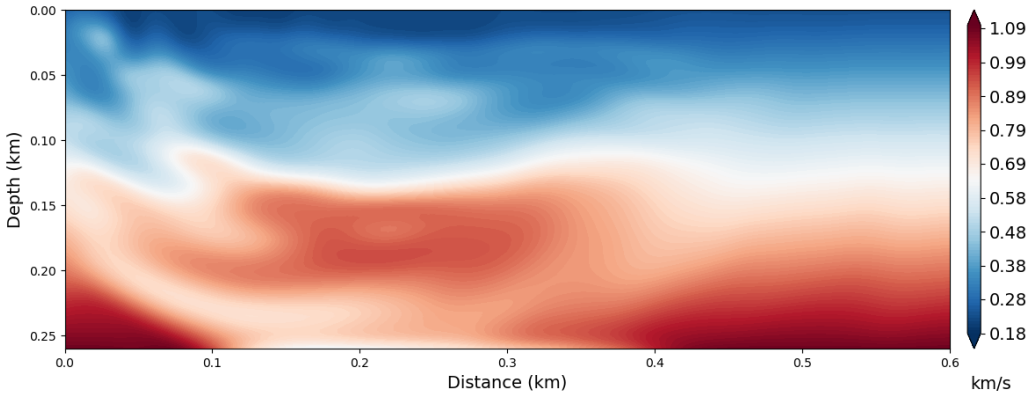

FIG. 12. Shear-wave velocity model obtained after FWI with envelop-difference misfit function.

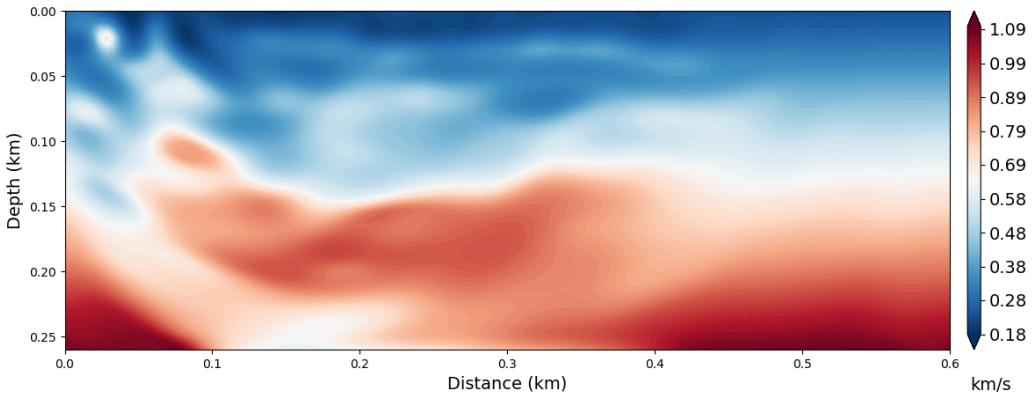

FIG. 13. Shear-wave velocity model obtained after FWI with waveform-difference misfit function.

synthetic data and observing data. We used 5 shots of straight-line fibreoptic data buried in the 1-meter deep trench. The recording fibre has a nominal gauge length of 10 m and trace spacing of 0.66 m. From the shot record and f-k analysis of the DAS data, strong energy of multimodal ground roll could be seen, while reflection and refraction waves can hardly be observed (FIG. 10 (a)). Other detailed information was illustrated in the report last year.

Since the multi-offset MASW has been conducted on the same dataset, a rough background shear-wave velocity can be obtained. The initial velocity model is a linear model built based on the shear-wave velocity obtained from the previous MASW result. We used the combined (ED+WD) FWI with a frequency decreasing multi-scale approach. FIG. 12 is the inversion result of envelop-based FWI, and FIG. 13 is the result of combined FWI. From these figures, we can find the general velocity structure within 200 m can be recovered. Some small shallow structures may be influenced by the noise in the data, while the large-scale structures should be reliable. Since the sources are placed in the upper-left corner, we can find the near-offset area has a higher resolution than the far-offset area.

CONCLUSION

The multi-offset MASW can deal with the subsurface structure with mild lateral variations. However, when strong lateral heterogeneity exists, the results obtained cannot be treated reliable. The resolutions of dispersion curves inversion are limited both in lateral and vertical directions. Even for the data containing rich low-frequency components, velocity structure inverted beyond 100 m in depth are quite uncertain. Besides, the accuracy of dispersion curves picking has a great influence on the inversion results. But the inverted velocity range is generally stable. Surface-wave FWI has advantages in resolving complex lateral heterogeneities. Besides, the resolution ability of FWI is much better than MOPA both in lateral and vertical directions. Thus, reliable velocity structures expanding to a deeper area can be obtained. Combined (ED+WD) FWI and frequency decreasing multi-scale inversion strategy is useful to minimize the cycle skipping. It is feasible to use the surface-trenched DAS data to conduct surface-wave FWI. Detailed structures expanding to deeper depth can be well recovered. To better improve the result, DAS simulation can be conducted for later study.

ACKNOWLEDGEMENTS

We thank the sponsors of CREWES for continued support. This work was funded by CREWES industrial sponsors, NSERC(Natural Science and Engineering Research Council of Canada) through the grant CRDPJ 461179-13 and CRDPJ 543578-19. Luping was partially supported by a scholarship from SEG. Thanks to the Containment and Monitoring Institute and all the field stuff for DAS data collection. Thanks also to Raul Cova for his generous sharing of surface wave data processing experience, to Zhan Niu for his helping in MPI running. Thanks to Don C. Lawton for providing background geology information of the DAS data.

REFERENCES

Bodet, L., Abraham, O., Bitri, A., Leparoux, D., and Côte, P., 2004, Effect of dipping layers on seismic surface waves profiling: a numerical study, *in* Symposium on the Application of Geophysics to Engineering and Environmental Problems 2004, Society of Exploration Geophysicists, 1601–1610.

Borisov, D., Modrak, R., Gao, F., and Tromp, J., 2018, 3d elastic full-waveform inversion of surface waves in the presence of irregular topography using an envelope-based misfit function: Geophysics, **83**, No. 1, R1–R11.

Bozdağ, E., Trampert, J., and Tromp, J., 2011, Misfit functions for full waveform inversion based on instantaneous phase and envelope measurements: Geophysical Journal International, **185**, No. 2, 845–870.

Cova, R., and Innanen, K., 2019, Full waveform inversion of multimode surface wave data: numerical insights, **volumn 31**.

Hall, K. W., and Lawton, D. C., 2019, Trace location assignment for the cami.frs fibre loop, **volumn 31**.

Luo, J., and Wu, R.-S., 2015, Seismic envelope inversion: reduction of local minima and noise resistance: Geophysical Prospecting, **63**, No. 3, 597–614.

Mastrocicco, M., Vignoli, G., Colombani, N., and Zeid, N. A., 2010, Surface electrical resistivity tomography and hydrogeological characterization to constrain groundwater flow modeling in an agricultural field site near ferrara (italy): Environmental Earth Sciences, **61**, No. 2, 311–322.

Pan, Y., Gao, L., and Bohlen, T., 2019, High-resolution characterization of near-surface structures by surface-wave inversions: From dispersion curve to full waveform: Surveys in Geophysics, **40**, No. 2, 167–195.

Romdhane, A., Grandjean, G., Brossier, R., Réjiba, F., Operto, S., and Virieux, J., 2011, Shallow-structure characterization by 2d elastic full-waveform inversion: Geophysics, **76**, No. 3, R81–R93.

Strobbia, C., and Foti, S., 2006, Multi-offset phase analysis of surface wave data (mopa): Journal of Applied Geophysics, **59**, No. 4, 300–313.

Vignoli, G., and Cassiani, G., 2010, Identification of lateral discontinuities via multi-offset phase analysis of surface wave data: Geophysical Prospecting, **58**, No. 3, 389–413.